A GCM Simulation of the Relationship between Tropical-Storm Formation and ENSO

GUOXIONG WU*

Program in Atmospheric and Oceanic Sciences, Princeton University, Princeton, New Jersey

NGAR-CHEUNG LAU

Geophysical Fluid Dynamics Laboratory/NOAA, Princeton University, Princeton, New Jersey

(Manuscript received 23 April 1991, in final form 23 September 1991)

ABSTRACT

A low-resolution Geophysical Fluid Dynamics Laboratory (GFDL) general circulation model has been integrated for 15 years. In the course of this experiment, the observed month-to-month sea surface temperature (SST) variations in the tropical Pacific Ocean were incorporated in the lower boundary condition. The output from this model run was used to investigate the influence of El Niño–Southern Oscillation (ENSO) events on the variability of tropical-storm formation.

Criteria for detecting tropical cyclogenesis and tropical-storm formation were developed for the model. Tropical storms appearing in the model atmosphere exhibit many typhoonlike characteristics: strong cyclonic vorticity and convergence in the lower troposphere, strong anticyclonic vorticity and divergence near the tropopause, and intense precipitation. It is demonstrated that, despite its coarse resolution, the model is capable of reproducing the observed geographical distribution and seasonal variation of tropical-storm formation.

The relationship between simulated tropical-storm formation and ENSO was explored using correlation statistics, composite fields for the warm and cold phases of ENSO, and individual case studies. Significant correlations were found between eastern equatorial Pacific SST anomalies and tropical-storm formation over the western North Pacific, western South Pacific, and western North Atlantic. In these areas, below-normal frequency of tropical-storm formation was simulated in warm El Niño years, whereas more tropical storms occurred in La Niña years. The correlation between tropical-storm formation and equatorial SST changes is particularly high for fluctuations on time scales of less than 3–4 years. During the boreal summer months (June–October), there exists a seesaw in the frequency of tropical-storm formation between western and central North Pacific: while more tropical storms were generated over western North Pacific during La Niña years, less tropical storms were detected over central North Pacific. The reverse situation prevails in El Niño years. Over the Indian Ocean, the relationship between storm formation and ENSO exhibits a seasonal dependence.

1. Introduction

During the last few decades, our knowledge of the structure, formation, movement, and prediction of tropical storms (abbreviated as TS hereafter) has expanded considerably. The progress in the research related to TS has been facilitated by the availability of satellite observations, as well as the dedication of numerous diagnostic and modeling efforts to this problem (for example, see Chen and Ding 1979; Anthes 1982; Wang and Fei 1987). It is now known that the formation of TS requires not only warm sea surface temperature (SST) and strong conditional instability in the lower troposphere but also favorable conditions in the environmental flow. During El Niño years, the difference in sea level pressure between the southeastern tropical Pacific and western Pacific reaches a minimum, and the tropical circulation undergoes dramatic changes (Rasmusson and Carpenter 1982; Rasmusson and Wallace 1983; Philander 1989). The dynamic and thermodynamic variations associated with ENSO exert a notable influence on TS activity. Reductions in TS formation during El Niño years over western North Pacific, western South Pacific, and western North Atlantic have been reported in a number of observational studies (Pan 1982; Chan 1985, 1990; Dong 1988; Li 1988; Nicholls 1984; Gray 1984a). However, in view of the multiple factors contributing to the formation of TS, it is difficult to isolate the impact of ENSO-related SST anomalies on TS activity by using observational data alone. Alternate approaches to this problem appear to be necessary.

The first attempt to simulate typhoon-type vortices

* On leave from the Institute of Atmospheric Physics, Chinese Academy of Sciences, Beijing, China.

Corresponding author address: Dr. Ngar-Cheung Lau, Princeton University, GFDL, P.O. Box 308, Princeton NJ, 08542.

by large-scale general circulation models (GCMs) was made by Manabe et al. (1970) at the Geophysical Fluid Dynamics Laboratory (GFDL). By using a global moist model with a horizontal grid spacing of 417 km, Manabe and his collaborators found good agreement between the observed and simulated sites of TS formation (see their Fig. 5.12). The capability of higher-resolution models to predict TS formation as well as to simulate the geographical and seasonal distributions of storm activity has also been demonstrated by Bengtsson et al. (1982). The ability of GFDL models to simulate the formation of TS was further assessed by the comprehensive study of Broccoli and Manabe (1990). Using multiyear integrations of GCMs with different resolutions, they found that the model-simulated TS resemble the corresponding observed systems in their thermodynamic structure. Moreover, the geographical distribution of the annual frequency of TS in their experiments is similar to the observed distribution.

Concurrently, the advances in our understanding of ENSO (for example, see Bjerknes 1966, 1969; Rowntree 1972; Philander 1989) have motivated many numerical experiments aimed at simulating this family of phenomena (e.g., Blackmon et al. 1983; Shukla and Wallace 1983; Palmer and Mansfield 1984; Wu and Cubasch 1987). The time-varying nature of the tropical Pacific SST forcing as well as the seasonality of the model response were incorporated explicitly in a series of GCM experiments reported by Lau (1985). The model analyzed in the latter study has nine levels in the vertical and uses a rhomboidal truncation at 15 wavenumbers. Variations in the tropical Pacific SST between 30°N and 30°S were updated every day using temporal interpolations from monthly observations for the 1962–76 period. In other parts of the World Ocean, climatological monthly mean SST data were used. By using this experimental design, Lau was able to reproduce the temporal evolution of individual ENSO episodes occurring in the 15-yr period.

Since the GFDL model is capable of producing TS-like features, and since the same model can simulate the essential characteristics of ENSO events with the incorporation of time-varying SST forcing in the lower boundary condition, it would be feasible to investigate the relationship between TS formation and ENSO by analyzing the appropriate model output from the experiments described by Lau (1985). Considering that the tropical Pacific SST changes provide the only external forcing on interannual time scales in that integration, the model data should reveal any correlation between TS formation and ENSO more clearly than observational data. The objective of the present study is to investigate the nature of such relationships in the model atmosphere. Suitable criteria for detecting TS formation are developed for the model in section 2. In section 3, the temporal and spatial characteristics of the simulated TS are examined. Composites of TS over the Western North Pacific are computed, and the typical structure of the simulated storms is described. The seasonal variation and geographical distribution of the frequency of TS formation in the model atmosphere are also documented. The relationships between ENSO and the genesis of TS over different oceans are then studied in section 4. Section 5 is devoted to the understanding of these relationships through the use of seasonal or monthly composites of selected fields for La Niña and El Niño events. Conclusions from this study and discussions on further work relevant to this subject are given in section 6.

2. Criteria for detecting tropical-storm formation

In the present model study, the daily output from the experiment described by Lau (1985) was analyzed. The meteorological fields examined include geopotential height at 200, 500, and 1000 mb, temperature and horizontal wind at 200 and 950 mb, water vapor mixing ratio at 950 mb, vertical velocity at 500 mb, and precipitation. The horizontal grid spacings of these model data are 7.5° of longitude and 4.5° of latitude. The following simple criteria have been used to identify cyclone systems at grid points L in the latitude zone between 40.5°S and 40.5°N:

- At 1000 mb, the geopotential height at L must be at a minimum relative to the eight surrounding points; the 950-mb circulation at L must be both cyclonic and convergent; and the 500-mb vertical motion at L must be directed upward.
- The thickness between 200 and 1000 mb over L must be at a maximum relative to the four neighboring points and must exceed (by 60 m) the corresponding mean value of the grid points lying within 1500 km to the west and east.
- The wind speed at 950 mb must exceed gale-force strength (i.e., 17.2 m s^{-1}) at one or more of the nine grid points in the proximity of L.

The systems satisfying these criteria will henceforth be referred to as *cyclones*. Since emphasis is placed on storm genesis, any cyclone that is located within a distance of 7.5° of longitude or 9° of latitude from a cyclone identified one day earlier will be regarded as the same cyclone having migrated from its previous location and will be excluded from this census.

The criteria listed above were applied on a day-to-day basis to the model output. During the 15-yr integration, there are altogether 10 011 surface cyclones detected in the domain under investigation. Figure 1a shows the geographical distribution of total number of cyclone formation at individual grid points. The latitudinal distribution of the frequency of cyclone formation is depicted in Fig. 1b. These results indicate that a substantial portion of the detected cyclones are located in extratropics, mainly in the winter season.

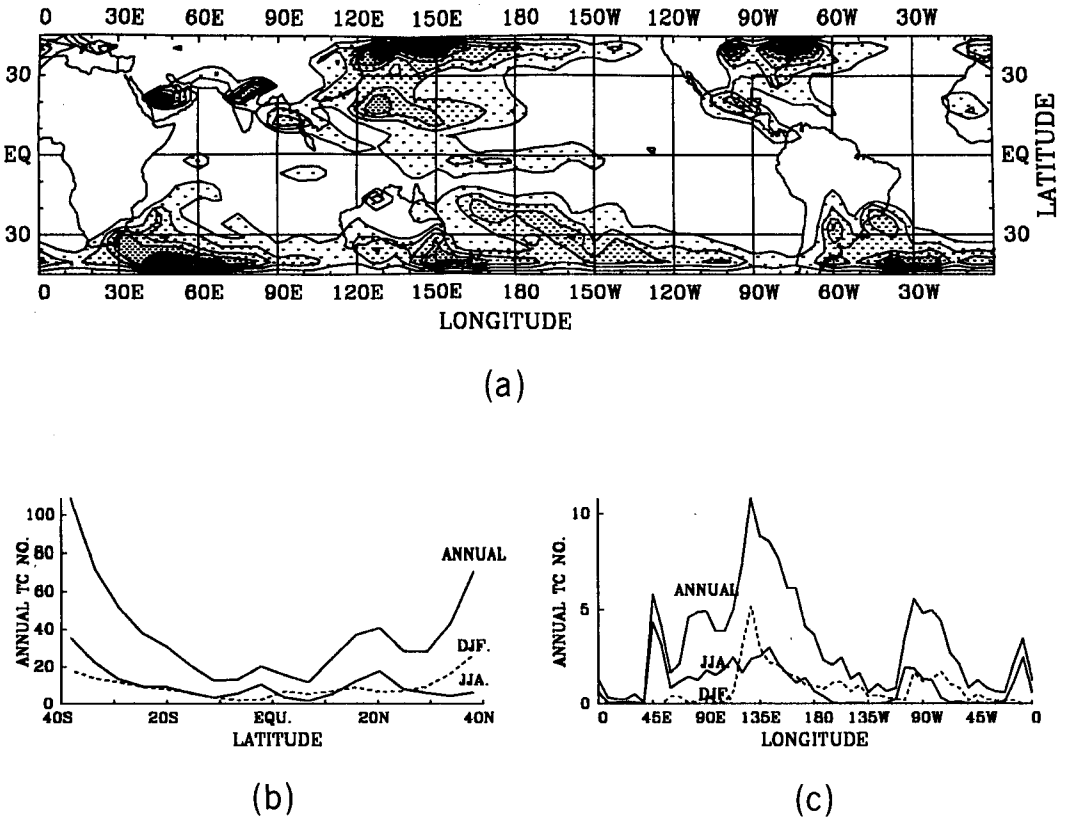

FIG. 1. (a) Distribution of the frequency of model-simulated cyclone formation at each 4.5° latitude × 7.5° longitude grid box. The values shown here correspond to the total number of occurrences of cyclone formation during the entire 15-yr integration. Annual frequency may hence be obtained by dividing these values by 15. Contour interval in 10. The contours plotted correspond to values of 10, 20, 30, and 40. Stippling with progressively higher densities is used to depict regions of frequent cyclone formation. Regions with more than 50 occurrences are indicated by solid black. (b) Latitudinal distribution of annual and seasonal cyclone frequencies summed over all longitudes. (c) Longitudinal distribution of annual and seasonal cyclone frequencies between 13.5° and 31.5°N.

Local maxima are also found near the equator and in subtropical regions. In the northern subtropics between 13.5° and 31.5°N, the longitudinal distribution of the frequency of cyclogenesis (Fig. 1c) is characterized by local maxima over western Africa, Saudi Arabia, Bay of Bengal, western North Pacific (WNP), and western North Atlantic (WNA) to the east coast of the United States. The frequencies in these regions are particularly high in summer.

Analysis of the seasonal variation of the simulated disturbances shows that the cyclones over western Africa, Saudi Arabia, and the Bay of Bengal mostly develop in summer months, whereas the systems over WNP and WNA occur every season. In order to differentiate TS from other types of disturbances, composite charts of the detected cyclone systems have been constructed for different areas and different seasons by the following procedure: the center of each of these cyclones was assigned as the origin of a common coordinate system, with the abscissa and ordinate corresponding to longitudinal and latitudinal displacement from the cyclone center, respectively. The model data within 30° of longitude (i.e., four grid points in the zonal direction) and 31.5° of latitude (i.e., seven grid points in the meridional direction) from each cyclone center were translated to this common frame of reference. Composite plots were then obtained by averaging the data over all cases in the common coordinate system. Some of the composite results are presented in Fig. 2.

At 38.25°N in January, the surface cyclone is typically associated with a cyclonic wave that is characterized by temperature perturbations lagging behind geopotential height perturbations (figures not shown) and by strong westerlies at 200 mb (Fig. 2a). The composite pattern of 200-mb wind for the WNP region in January (Fig. 2b) resembles that pertaining to 38.25°N. These systems should therefore be classified as baroclinic disturbances. On the other hand, the composite for WNP in July is very different from its wintertime counterpart and bears many distinct TS characteristics, with a geopotential low at 500 mb, an anticyclone at 200 mb,

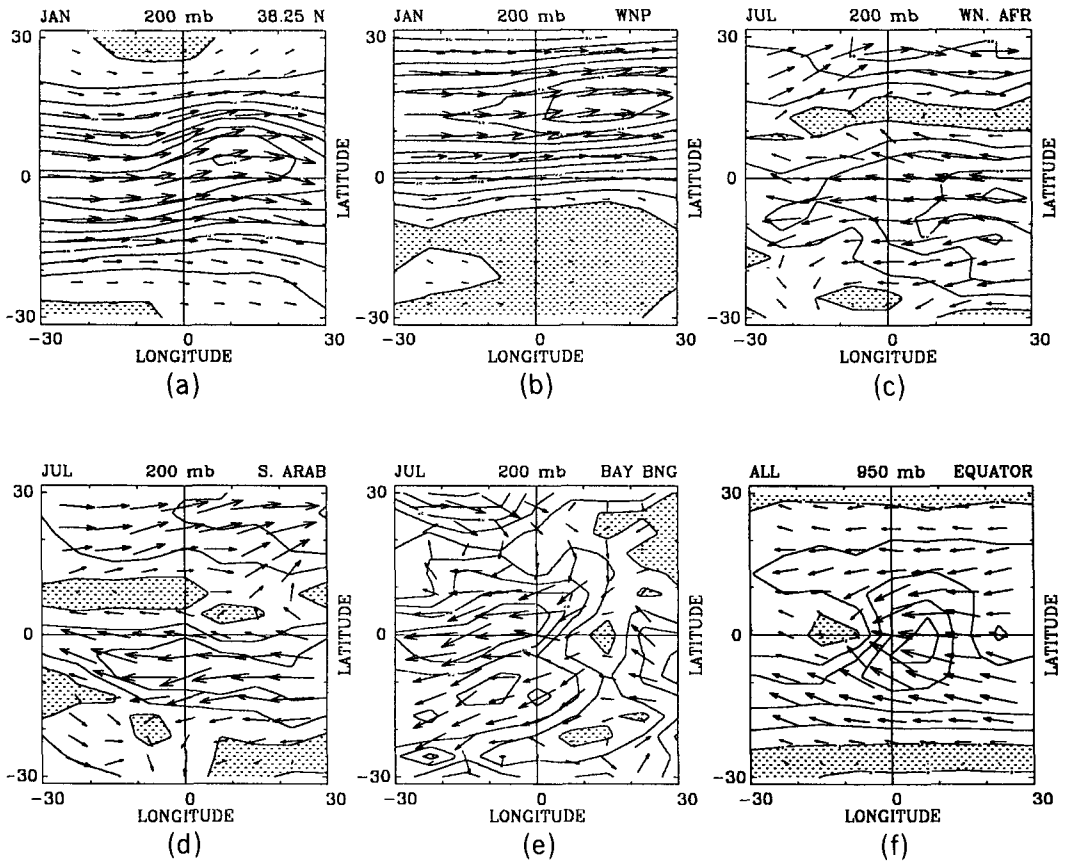

FIG. 2. Composites of velocity vectors at 200 mb [(a)–(e)] and at 950 mb [(f)] for cyclones identified in different seasons and different areas (see text for details of composite procedure). Contours indicate wind speed at intervals of 5 m s^{-1} at 200 mb and 2 m s^{-1} at 950 mb. Stippling indicates wind speeds less than 5 m s^{-1} at 200 mb and 2 m s^{-1} at 950 mb. Panel (a) is for 38.25°N in January; Panel (b) is for WNP in January; Panel (c) is for western North Africa in July; Panel (d) is for southern Saudi Arabia in July; Panel (e) is for the Bay of Bengal in July; and Panel (f) is for the equatorial belt between 4.5°S and 4.5°N and for all seasons.

and very weak wind speed directly above the surface low (refer to Fig. 3).

The July composites for western Africa, Saudi Arabia, and the Bay of Bengal (Figs. 2c–2e) are all characterized by strong 200-mb easterlies directly above the surface-low center. Composites of water vapor mixing ratio at 950 mb for western Africa and Saudi Arabia (figures not shown) indicate very dry conditions. These results suggest that the perturbations over western Africa are cyclonic systems developing along the north African dry baroclinic zone, as noted by Carlson (1969) and Burpee (1974).

In the equatorial zone, the disturbances mainly occur to the east of the "maritime continent" in the western Pacific (Fig. 1a). The composite pattern of the 950-mb wind field (Fig. 2f) shows that most of the equatorial perturbations do not resemble TS, since they are characterized by surface easterlies on both the northern and southern flanks of the disturbance center. This rather unique flow pattern allows the equatorial systems to be distinguished from other disturbances.

It is evident from the composite patterns shown in Fig. 2 that the cyclonic systems generated in the model include not only TS, but also baroclinic cyclones, continental dry cyclones, and equatorial easterly perturbations. On the basis of this evidence, the following additional constraints were applied to each of the cyclones detected earlier so as to retain only those systems with TS characteristics:

1) The 200-mb zonal wind above the cyclone center L must not exceed 5 m s^{-1} (westerly).
2) The 950-mb relative humidity at L must exceed 70%.
3) The 950-mb zonal wind component must not be easterly at both the grid point located 4.5° to the north and the point located 4.5° to the south of L.

Experimentation with different thresholds indicates that the results are not sensitive to the particular cutoff values chosen above. The impact of the additional

constraints on the distribution of the frequency of cyclogenesis has been evaluated by comparing the pattern in Fig. 1 with the corresponding patterns obtained by incorporating the new constraints one at a time (not shown). As expected, the first constraint serves to exclude baroclinic perturbations. The second constraint effectively removes tropical continental dry disturbances, particularly those located over western Africa and Saudi Arabia. The third constraint removes those equatorial easterly disturbances possessing the structure noted in Fig. 2f. As will be demonstrated in the next section, the application of these additional constraints makes retention of only those typhoonlike systems possible, resulting in a realistic seasonal and spatial distribution of the frequency of TS formation.

The selection criteria developed in the present study may be compared with those implemented in Broccoli and Manabe (1990), who have analyzed various versions of essentially the same GCM. Both studies require the surface pressure at the storm center to be at a minimum and the wind speed in the vicinity of the storm to exceed gale-force strength. Broccoli and Manabe (1990) excluded most of the baroclinic cyclones by considering only grid points equatorward of ~30° latitude, and by conducting the search only during a 6-month hurricane season, which corresponds to the warm half of the annual cycle. They have also eliminated the continental dry cyclones from their census by surveying only the oceanic grid points. The differences between the two detection procedures notwithstanding, the gross spatial characteristics of the frequency of TS occurrence as reported in both studies are in fair agreement with the observations (see Broccoli and Manabe 1990, Table 1; and section 3 of this paper).

3. Model climatology of TS formation

In order to ascertain that the criteria and constraints developed in the preceding section are appropriate for identifying circulation systems with TS characteristics, the composite TS structure in the WNP area will be examined in this section. The geographical and seasonal variations of simulated TS formation will also be documented. The model results presented here will be compared with observational data.

While assessing the realism of the model results presented here, the fact that the cyclones are generated by a GCM with very low spatial resolution (i.e., rhomboidal truncation at only 15 wavenumbers) should be kept in mind. It is anticipated that this model is not capable of reproducing the fine details of the mesoscale cyclone structure. Therefore, this study will concentrate on those aspects of the tropical storms with spatial scales longer than that resolvable by the model grid. The prediction experiments performed by Krishnamurti et al. (1989) offer ample evidence linking increased model resolution with improved forecast skill of TS formation, movement, and structure. Hence, the findings reported here need to be further validated by analyzing model runs with higher resolution. It is, however, noteworthy that the regional climatology of TS occurrence in the 15-wavenumber model is not notably different from that in a 30-wavenumber model (see Broccoli and Manabe 1990).

a. Composite TS structure over WNP

Altogether, 128 storms were identified over WNP (0°–45°N, 101.25°–168.75°E) in the summer months of July, August, and September in the 15-yr model integration. The composites of the horizontal wind vector, relative vorticity, and divergence fields at 200 and 950 mb, and the geopotential height fields at 200 and 1000 mb are shown in Fig. 3. The same composite procedure described in the previous section has been used to construct these patterns. At the lower level there is a distinct region of convergence surrounding the storm center, with a radial extent of about 1000 km (Fig. 3f), as well as a core region of cyclonic relative vorticity surrounded by anticyclonic vorticity (Fig. 3d). The horizontal circulation exhibits a notable degree of asymmetry about the storm center, with southerlies in the eastern sector being much stronger than the northerlies to the west (Fig. 3b). The polarities of the composite vorticity and divergence fields at the upper level are opposite to those at 950 mb. The 200-mb circulation over the storm is characterized by anticyclonic vorticity (Fig. 3c), divergence (Fig. 3e), and wind vectors spiraling out of the vortex center (Fig. 3a). A low geopotential center appears at 1000 mb (Fig. 3h), with gradients to the west being noticeably weaker than those to the east and north. The asymmetric structure of the low-level depression is similar to that observed in the Northern Hemisphere (Shea and Gray 1973) and is related to the ambient circulation in the western North Pacific. In that region there exists a semipermanent subtropical high pressure center to the northeast of the site of storm formation, whereas a quasi-stationary monsoon low system prevails to the west. This spatial configuration of the mean-flow environment agrees well with observations (Ding and Reiter 1981). The average depth of the simulated TS in terms of D value for the geopotential height field at 1000 mb (which is defined as the difference between the height or pressure value at the low center and the mean value at the two grid points located at 1500 km to the east and west of the center, see Frank 1977) is −70 m (or −9 mb), about half of the corresponding observed amplitude as reported by Frank. The low center becomes weaker with increasing height: the D value at 500 mb is only −24 m, or about −2 mb. At 200 mb (Fig. 3g), a high geopotential center with a D value of +26 m appears. In reality, the sign reversal in the geopotential height field for a TS over WNP usually occurs above 200 mb (Frank 1977). The present results suggest that the ver-

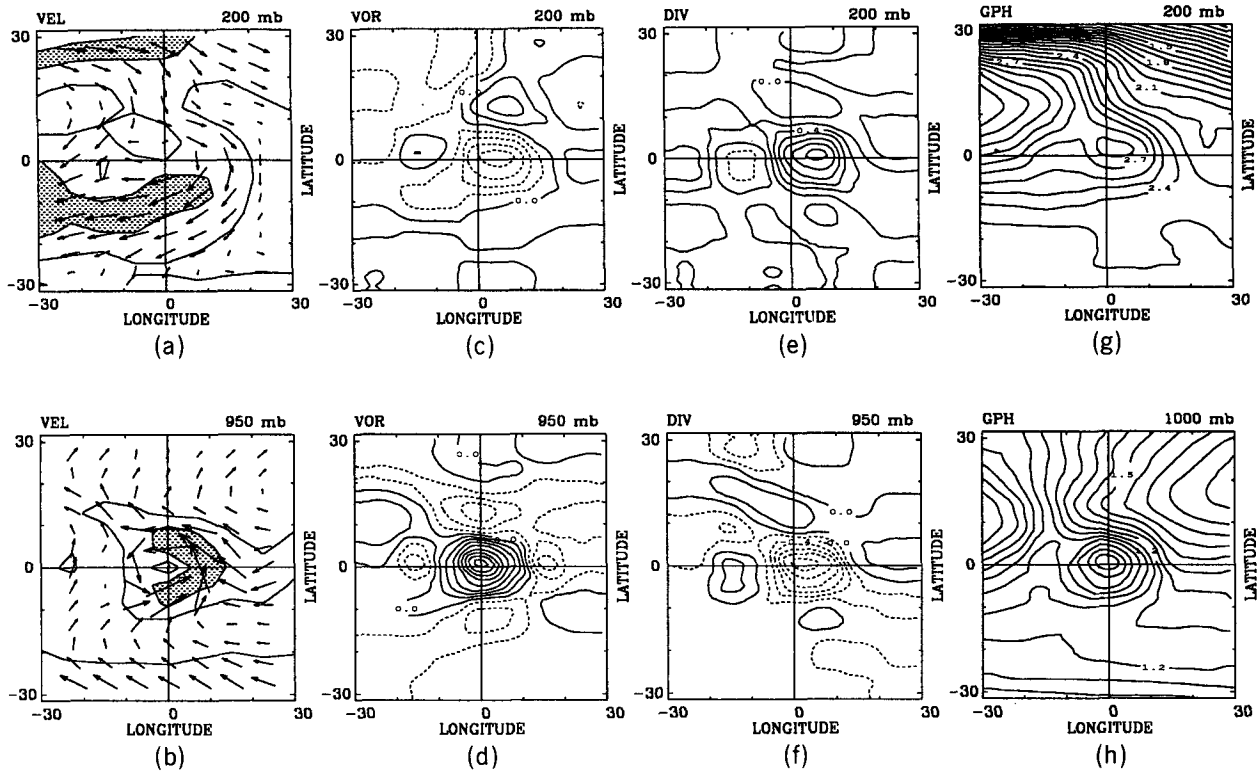

FIG. 3. Composite patterns of the model data at 200 mb (upper panels), 950 mb [(b), (d), and (f)], and 1000 mb (h) for (a) and (b) horizontal wind, contour interval in 5 m s^{-1}, stippling indicates wind speed larger than 10 m s^{-1}; (c) and (d) relative vorticity, contour interval in 5×10^{-6} s^{-1}, dashed contours indicate negative vorticity; (e) and (f) divergence, contour interval in 2×10^{-6} s^{-1}, dashed contours indicate convergence; and (g) and (h) geopotential height, the contour values at 200 mb have been subtracted by a constant value of 12 200 m, contour interval in 10 m.

tical extent of the simulated storm is shallower than that observed. The lower level of the TS is also characterized by high moisture content, strong upward motion, and heavy precipitation with rates reaching 34 mm day^{-1} (figures not shown). Numerical experiments on typhoon formation with a fine-mesh model by Kurihara and Tuleya (1981) show that maximum rainfall rates of 48–72 mm day^{-1} can be produced on the first day of storm formation.

The amplitudes of the model patterns displayed in Fig. 3 are generally lower than those documented by Frank (1977) for observed cyclones, thus implying that the present low-resolution model tends to underestimate the storm intensity. However, it is also evident from the composites that the TS generated in the present model exhibit considerable qualitative similarities to their observed counterparts.

b. Regional distribution of TS

Figure 4a shows the geographical distribution of the frequency of TS formation at individual grid points during the 15-yr model integration. The pattern in Fig. 4a bears some resemblance to the corresponding distribution in the real atmosphere (Fig. 4b), as presented by Gray (1979). For both the observed and simulated atmospheres, TS mainly develops over the oceans. There are more TS generated in the Northern Hemisphere than in the Southern Hemisphere. The Bay of Bengal and the region east of the Philippines over the western Pacific Ocean are the most favorable regions for TS formation. The occurrence of TS formation near the Brazilian coast in the model atmosphere does not appear to be supported by the available observations. Other sites of storm formation include WNA, western South Pacific, and the southern Indian Ocean. No storm occurs over the eastern South Pacific and eastern Atlantic, where the circulation is dominated by subtropical high pressure centers, with prevalent large-scale subsidence.

Over the southern central Pacific, the area of enhanced TS formation in the model extends farther to the east. This eastward shift is consistent with the corresponding displacement of the South Pacific convergence zone (SPCZ) in the model from the observed position (see Lau 1985, Fig. 3). The TS formation over WNA in the model is less evident than that in the observations. This discrepancy may be related to the fact that the simulated 200-mb trough in the Atlantic sector is displaced too far west of its observed position (see Lau 1985, Fig. 4b). Accordingly, the climatological

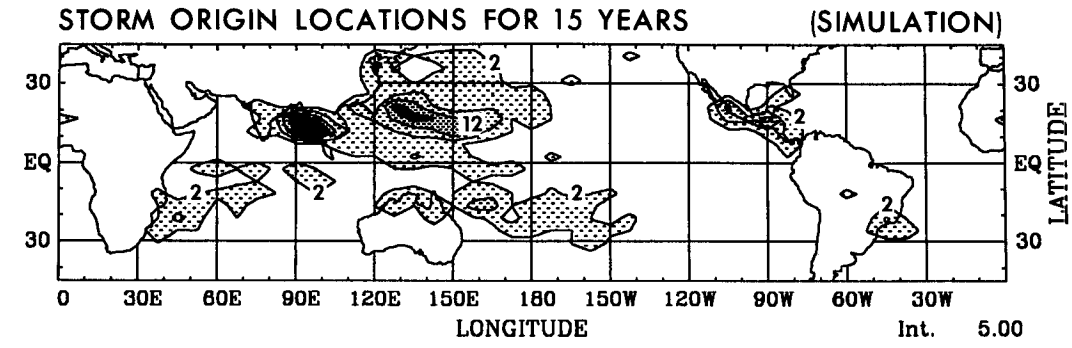

(a)

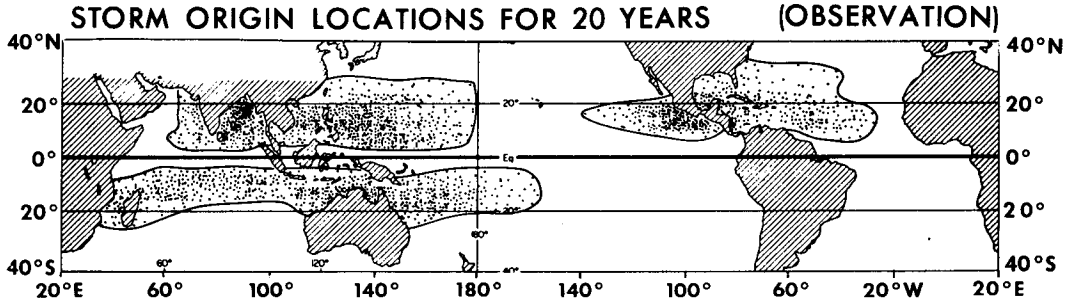

(b)

FIG. 4. Geographical distribution of the formation of tropical storms in the (a) simulated and (b) observed atmospheres. The model pattern depicts the total number of occurrence of storm formation during the entire 15-yr integration. Values with the ranges of 2–7, 7–12, and 12–17 are depicted by light, medium, and dense stippling, respectively. Regions with more than 17 occurrences are indicated by solid black. The observed pattern is reproduced from Gray (1979) and depicts the locations of individual storm cases during a 20-yr period.

North Atlantic tropical anticyclone at 200 mb in the model also shifts westward, thus inhibiting the formation of storms in the central Atlantic.

The overall agreement in the geographical distribution of TS between model and observation is encouraging. To further evaluate the model capability in simulating the spatial dependence of storm formation, the global ocean was divided into ten regions, that is, northern and southern Indian Ocean (NIO, 33.75°–101.25°E; SIO, 18.75°–123.75°E), WNP (101.25°–168.75°E), western South Pacific (WSP, 123.75°E–131.25°W), central North Pacific (CNP, 168.75°E–138.75°W), eastern North and South Pacific (ENP, 138.75°W to the west coast of the United States; ESP, 131.25°–63.75°W), WNA (east coast of the United States to 26.25°W), eastern North Atlantic (ENA, 26.25°–3.75°W), and South Atlantic (SAT, 63.75°W–18.75°E). The latitudinal extent of these regions is from the equator to 45°N and 45°S for the northern and southern regions, respectively. The mean annual frequency of TS formation in each ocean region was evaluated, and the results are compared to the corresponding observations (Gray 1968) in Table 1. In view of the systematically weaker TS intensities simulated in this low-resolution model (see section 3a), it may not be too meaningful to compare the actual number of observed and modeled storms satisfying a similar set of selection criteria. Instead, the frequency of TS formation in a given region has been expressed as a fraction (in percent) of the total number of TS occurring throughout the globe. These relative frequencies have been computed separately for the model and observed

TABLE 1. Simulated and observed mean annual frequency of tropical-storm formation in different regions. The observations are from Gray (1968).

Area		Modeled		Observed	
Ocean	As defined by Gray	Number	Percentage	Number	Percentage
NIO	III + IV	8	11	8	13
WNP + CNP	II	31	44	22	36
ENP	I	5	7	10	16
WNA	VIII	3	4	7	11
ENA		1	1		
SIO	V	8	11	6	10
WSP	VI + VII	13	18	9	14
SAT		2	3	0	0
Total		71	99	62	100

atmospheres and are also shown in Table 1. The high percentages of storm events over WNP and WSP and the near absence of storms over SAT are reproduced in the model statistics. The percentages of simulated TS formation over WNP and WSP are somewhat too high. The percentages over other oceans, especially over ENP and WNA, are lower than the observations. It should be pointed out that, due to inaccuracies in the earlier part of the observational record, the number of observed hurricane occurrences presented in Table 1 may be lower than reality (see Gray 1977; Anthes 1982). The inclusion of satellite observations indicates that the annual number of hurricane occurrences is approximately 80 (Frank 1987).

In Table 2, the percentage of the total TS occurring in different latitude belts in the model is compared to that in the real atmosphere (Gray 1968). In both the model and observed atmospheres, most TS are generated in the subtropical latitude belt, with only about one-eighth of all TS forming to the north of the Tropic of Cancer.

c. *Seasonal variation of TS*

In Fig. 5, the seasonal variations of the maximum and minimum frequency of TS formation over WNP and CNP within the 15-yr integration period are shown together with the corresponding observations (Chen and Ding 1979). In the observed and model atmospheres, both maximum and minimum frequencies attain peak values in the summer months, whereas no TS is detectable from November to May in some years.

The hemispheric averages of the simulated frequency of TS formation for individual calendar months are presented in Fig. 6a. Note that the time axis for the Northern Hemisphere values is shifted with respect to the Southern Hemisphere data by 6 months, so as to align the two sets of statistics to the same phase of the seasonal cycle. In both hemispheres, maximum TS formation occurs in summer, and minimum TS formation is simulated in late winter or early spring. This gross feature is similar to the observations shown in Fig. 6b. In the winter half year, the model produces more TS than the real atmosphere. As a result, the amplitude of seasonal variation in TS frequency in the model is weaker than that inferred from the observations.

TABLE 2. Fraction of tropical storms occurring in different latitude belts. Storm formation in all months of the year has been considered. The observations are from Gray (1968). The model results are based on the ratios of the number of storms detected in various zones to the total number (see data given in parentheses).

Modeled		Observed
9°–18°N and 9°–18°S	9°–22.5°N and 9°–22.5°S	10°–20°N and 1°–20°S
48%	64%	65%
(511/1063)	(683/1063)	
	>22.5°N 14% (154/1063)	>22°N 13%

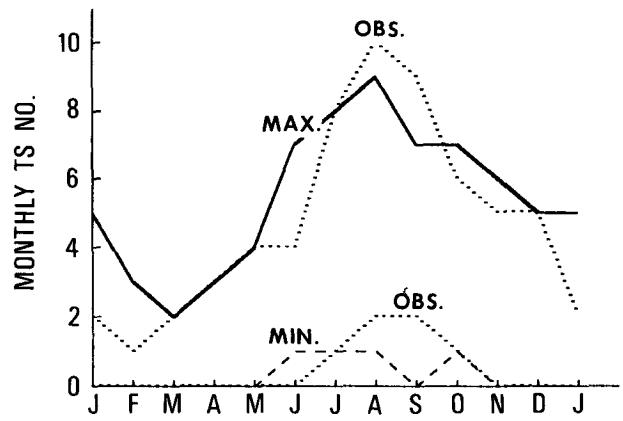

FIG. 5. Seasonal variation of the highest (solid curve) and lowest (dashed curve) frequency of storm formation over the western and central North Pacific for individual calendar months in the 15-yr simulation. The corresponding observed values are indicated by dotted curves.

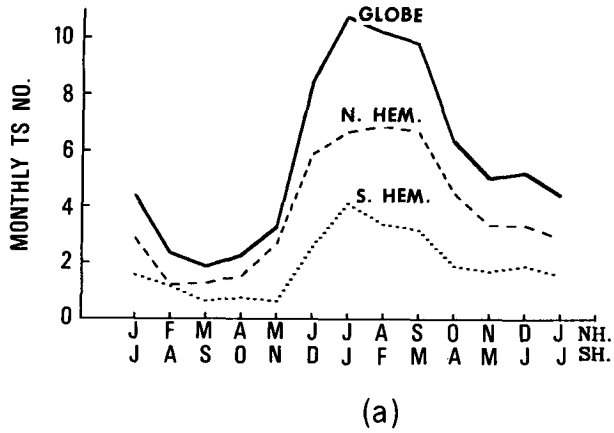

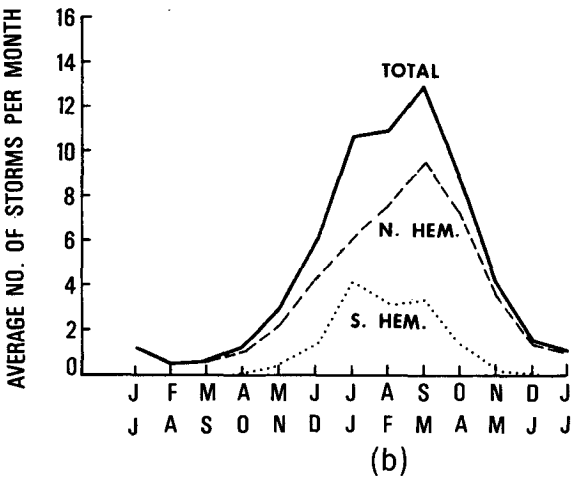

FIG. 6. Seasonal variation of the mean frequency of tropical-storm formation in individual calendar months, for the entire globe (solid curve), Northern Hemisphere (dashed curve), and Southern Hemisphere (dotted curve). The results are presented separately for the (a) model and (b) observed atmospheres. Note the 6-month shift in the time axes used for presenting the data in the two hemispheres.

4. Modulation of frequency of TS formation by ENSO events

a. Definition of El Niño and La Niña

In order to delineate the impact of ENSO-related variability on TS formation, the SST average over an appropriate portion of the equatorial Pacific will be used as an ENSO index. In Fig. 7, two time series of monthly and regional mean SST anomaly are presented. The anomaly for each month is defined as the deviation of the monthly mean from the 15-yr average of the corresponding calendar month. The dashed curve is based on area averages for the central equatorial Pacific (4.5°S–4.5°N, 176.25°E–138.75°W).

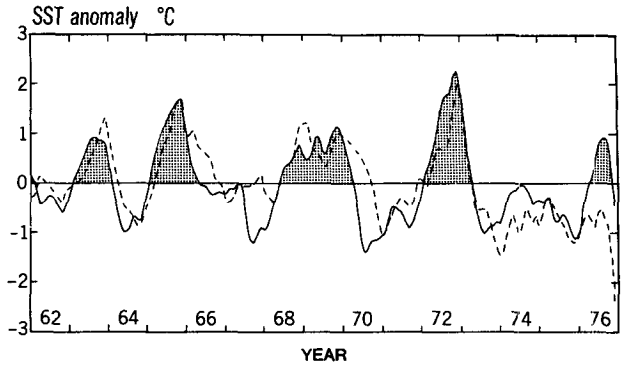

FIG. 7. Variation of observed SST anomalies in the central equatorial Pacific (dashed curve) and in the eastern equatorial Pacific (solid curve). Stippling denotes El Niño episodes determined using the SST data for the eastern equatorial Pacific.

The solid curve denotes the SST anomaly in the eastern equatorial Pacific (9°S–0°, 138.75°–86.25°W). The gross features of these two curves are rather similar, with the exception of 1976, during which the warming is confined to the vicinity of the Peru–Ecuador coast. In order to conform with other observational ENSO studies (e.g., Angell 1981; Rassmuson and Carpenter 1982), the eastern equatorial Pacific SST anomaly is used here to define the warm events. Altogether five warm ENSO events, that is, 1963, 1965, 1968/69, 1972, and 1976 (shown by stippling in Fig. 7) can be identified. For the cold La Niña events, the SST anomalies in both the eastern and central equatorial Pacific are considered. Four cold episodes, that is, 1964, 1967, 1970/71, and 1973–75, can be identified during the 15-yr period. In the following discussion, the SST anomaly over the eastern equatorial Pacific will be used as an index of ENSO.

b. Relationship between frequency of TS formation and ENSO

The relationship between global frequency of TS formation and ENSO will be assessed first. The model frequency of TS formation in individual years is ob-

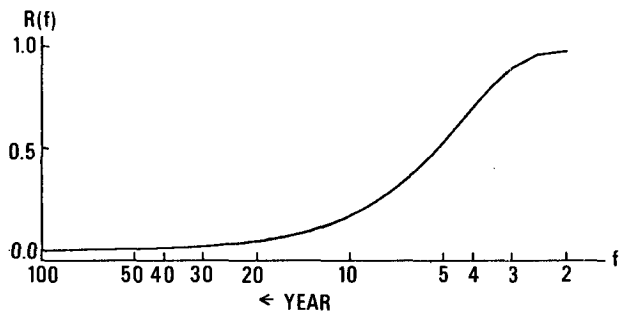

FIG. 8. Frequency response of the high-pass filter used in this study.

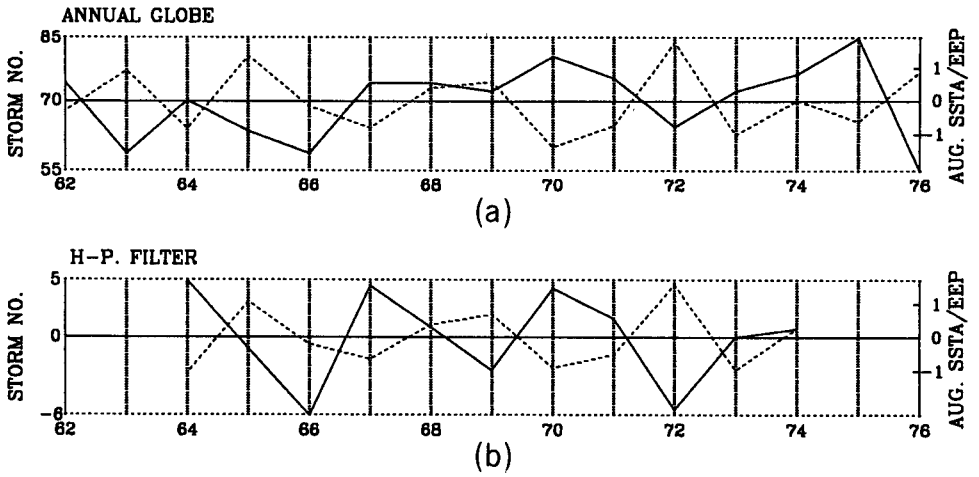

FIG. 9. (a) Variation in the annual frequency of simulated tropical-storm formation over the globe (solid curve) and observed August SST anomaly in the eastern equatorial Pacific (dashed curve). (b) As in (a), but for high-pass-filtered storm frequency and SST indices.

tained by the census described in section 2 and correlated with the August values of the SST anomaly in the eastern equatorial Pacific. The August SST anomaly is chosen because this month corresponds to the developing phase of most El Niño events in the 1962–76 period (Rasmusson and Carpenter 1982; Lau 1985). Assuming that the data values for individual years are mutually independent, the 95% and 99% significance limits for the correlation coefficients are estimated to be .51 and .64, respectively. Preliminary analyses show that both high- and low-frequency variations exist in TS frequency and in SST anomaly. Since this study's main emphasis is on the events with ENSO time scale, the fluctuations with that time scale have been retained by a high-pass filter. Following Holloway (1958), a five-point Gaussian filter has been designed to differentiate ENSO events occurring on time scales less than approximately 5 years from the much more slowly varying variations. The frequency response of this filter is presented in Fig. 8. This filter has been applied to the time series of both TS frequency and SST anomaly.

Figure 9 shows the time series of SST anomaly in the eastern equatorial Pacific and the annual mean frequency of TS formation for all oceans. The correlation coefficients for the unfiltered (Fig. 9a) and filtered (Fig. 9b) cases are −.65 and −.67, respectively, and are both above the 95% significance limit. The frequency of TS formation is below normal in most warm events and above normal in most cold events. This relationship is more evident in the high-pass-filtered data shown in Fig. 9b. Correlation analyses have also been performed for individual oceans and different seasons of the calendar year. Some of the results obtained from the filtered data are shown in Table 3. With the exception of the values for ENP, ENA, SIO and NIO, and the summertime value for WSP, the correlation coefficients are mostly negative, that is, less (more) TS are generated in El Niño (La Niña) years. Within the period of May–November, the negative correlations between ENSO and TS formation over WNP, WSP, and WNA are all above the 95% confidence level. Figures 10 and 11 present the variations of frequency of TS formation in individual oceans in relation to the eastern equatorial Pacific SST. The model results summarized here may be compared with observational analyses for the following individual regions.

1) WNP (FIG. 10a) AND CNP (FIG. 10b)

The strongest negative correlation between TS formation in the model and ENSO is found in WNP. Except for the period between January and March, the

TABLE 3. Correlation coefficients between August SST anomaly in the eastern equatorial Pacific and frequency of tropical-storm formation in different seasons and different oceans. The time series have been processed through a high-pass filter. Italics denotes values exceeding the 95% significance level.

	Globe	WNP	WSP	ENP	WNA	ENA	SAT	NIO	SIO
December–April	−.04	*−.88*	.21	.27	.23	.00	−.17	−.37	.38
May–November	*−.61*	*−.70*	*−.62*	.21	*−.69*	.19	−.15	.57	.04
Annual	*−.67*	*−.78*	−.11	.30	−.55	.19	−.20	.54	.23

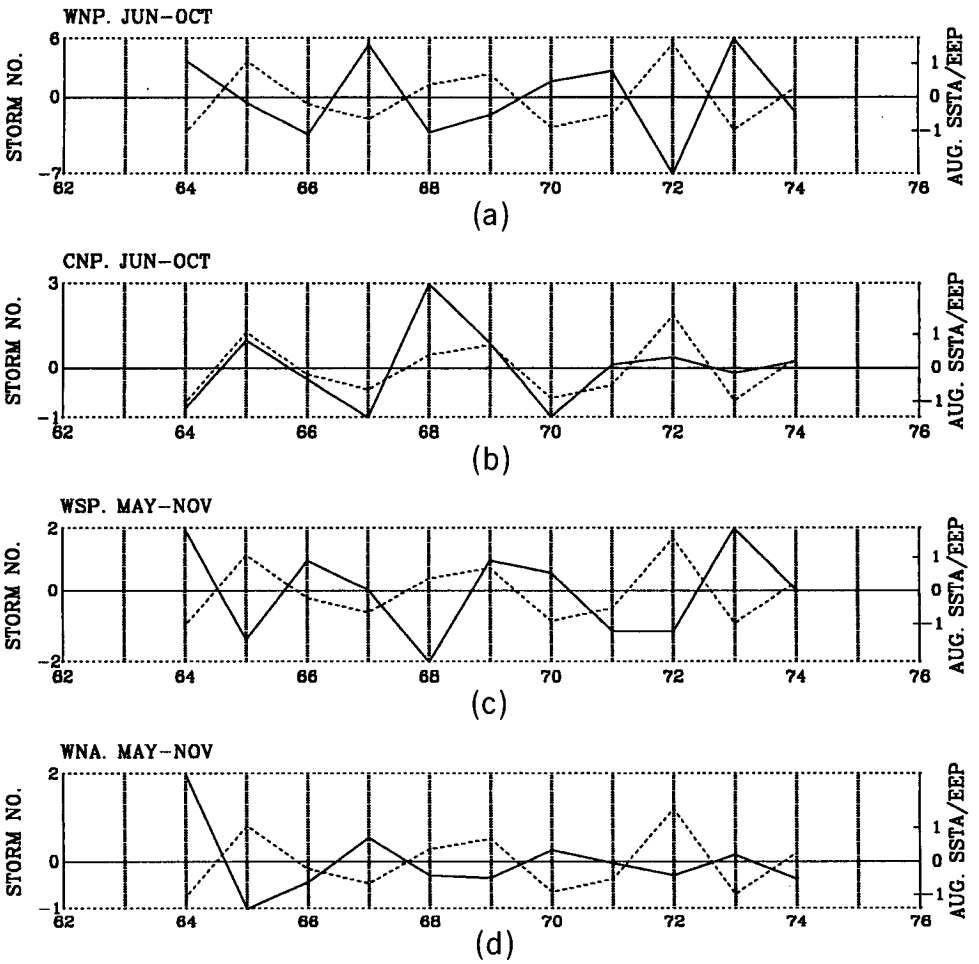

FIG. 10. Variation in the frequency of simulated tropical-storm formation in summer months over different oceans (solid curves) and observed August SST anomaly in the eastern equatorial Pacific (dashed curves). The storm frequency and SST indices have been processed through a high-pass filter. Panel (a) is for WNP between June and October; Panel (b) is for CNP between June and October; Panel (c) is for WSP between May and November; and Panel (d) is for WNA between May and November.

negative correlation coefficients for other seasons are all above the 95% confidence level. Correlation analyses have been performed for the summer period between June and October in different longitudinal domains in the region (Table 4). Negative correlations are obtained in every longitudinal domain west of 168.75°E, with the strongest negative correlation coefficient reaching −.89 for the region between 146.25° and 168.75°E. On the contrary, significant positive correlation is found over the central North Pacific (168.75°E–138.75°W). Therefore, a seesaw in TS formation between WNP and CNP occurs in the model in response to ENSO: during El Niño years, while WNP experiences less TS formation, more TS are generated over CNP. The reverse situation holds for La Niña years.

Using observational data of the 1948–82 period, Chan (1985) found that the spectra of both TS frequency in the WNP and the Southern Oscillation index

TABLE 4. Correlation coefficients between August SST anomaly in the eastern equatorial Pacific and frequency of tropical-storm formation during the summer months (June–October) in different longitudinal domains of the western and central North Pacific. The time series have been processed through a high-pass filter. Italic and bold numbers denote values exceeding the 95% and 99% significance levels, respectively.

Longitude	101.25°–123.75°E	123.75°–146.25°E	123.75°–168.75°E	146.25°–168.75°E	168.75°E–138.75°W
Correlation coefficient	−.40	*−.61*	**−.78**	**−.89**	*+.63*

peak in the 3–3.5-yr frequency band, and that the cross spectrum of these two indices has significant coherence on this time scale. Chan (1990) also found that the number of TS is below normal in the western part of WNP during El Niño years. At the same time, more TS tend to develop in the eastern part of that region. Based on data for the 1900–79 period, Li (1988) reported a significant correlation between ENSO and typhoon occurrence in WNP. His results indicate that the mean annual number of typhoon occurrence in WNP (excluding South China Sea) increases from 21.4 for El Niño years to 26.2 for La Niña years. Dong (1988) also found negative and positive correlations between TS frequency and eastern Pacific SST anomaly for the regions located west and east of 160°E, respectively. These results are well represented in the model. On the other hand, by only considering strong El Niño events in the 1955–79 period, Ramage and Hori (1981) did not find any significant correlation between storm frequency and ENSO. However, it is worth noting that not all El Niño and La Niña events in this period were considered in Ramage and Hori's study. Hence, it is difficult to reconcile their findings with the present results.

2) WSP (FIG. 10c)

A significant negative correlation coefficient (−.62) between the model TS formation and ENSO in this region is found only for the period between May and November. Based on observational data for the 1950–74 period, Nicholls (1979) reported a negative correlation between the Darwin June–August sea level pressure and the TS frequency over the "cyclone area" (5°–35°S, 105°–165°E). On analyzing the data for 1913–37 and 1964–82, Nicholls (1984) found that the number of TS over this particular area exhibits negative correlations with the eastern Pacific SST and Darwin pressure from well before the start of the cyclone season to well into the season (October to April). This relationship is particularly strong in the early part of the cyclone season (October–December). The correlations are much weaker during the middle and late cyclone season (December–April). These observational results are well represented by the model as well. It is evident from Fig. 10c and Table 3 that the correlation coefficient in the southern winter and spring months is significantly negative, whereas that in the southern summer months becomes weakly positive.

3) WNA (FIG. 10d)

The negative correlation between the variations of the model TS frequency in the western North Atlantic in summer months and the eastern equatorial Pacific SST anomaly is significant and comparable to that in WNP. In the real atmosphere, the relation between hurricane occurrence over the Atlantic and ENSO events seems to be more complicated (see Gray 1984a, 1984b; and Gray et al. 1987). However, the latter studies do show a negative correlation between TS frequency and ENSO.

4) NIO AND SIO (FIG. 11)

From the unfiltered model results, no significant correlation between TS formation and ENSO can be identified in the Indian Ocean in any period of the calendar year. This model finding is in agreement with observational results (see Mandal 1989). However, the filtered data show that the TS variations in the NIO region may be correlated with the SST index. The correlations exhibit a strong seasonal dependence (Table

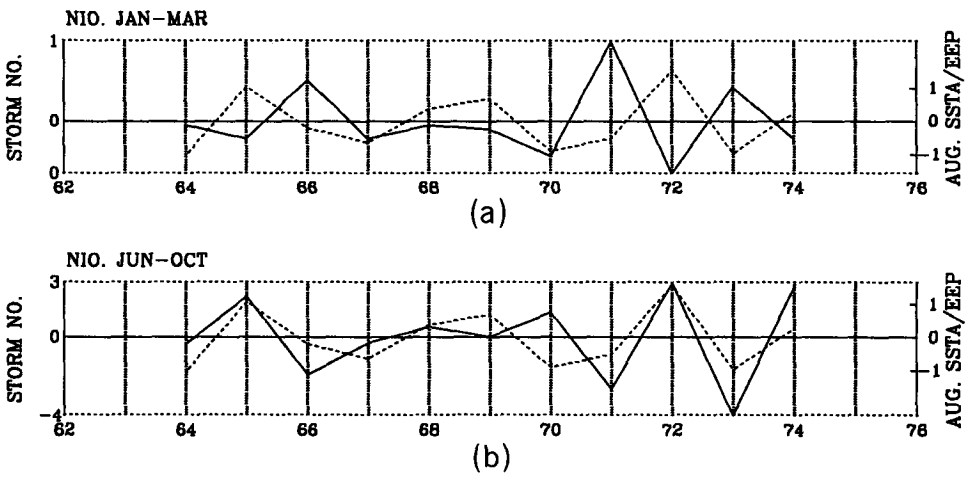

FIG. 11. Variation in the frequency of simulated tropical-storm formation over north Indian Ocean (solid curves) and observed August SST anomaly in the eastern equatorial Pacific (dashed curves). The storm frequency and SST indices have been processed through a high-pass filter. Panel (a) shows January–March, and Panel (b) shows June–October.

3). Weakly negative correlation (−.44) is found in the winter months of January to March (Fig. 11a), whereas significant positive correlation (+.65) is found in the summer months of June–October (Fig. 11b), when the monsoon trough migrates over the Bay of Bengal.

In the last decade, many efforts have contributed to expanding our observational knowledge of the relationship between Indian monsoon rainfall and ENSO events (e.g. Angell 1981). Strong negative correlations between Indian monsoon rainfall and warm ENSO events have been reported, for example, by Shukla and Paolino (1983), and Rasmusson and Carpenter (1983). These authors also noted that the precipitation anomaly over Sri Lanka and extreme southern India is different from the anomaly in the interior of the Indian subcontinent. For instance, above-normal precipitation in the former regions were observed during the autumn of the warm episode. As most of the TS in NIO occur in the Bay of Bengal (see Fig. 4), the monsoon rainfall over much of the Indian subcontinent

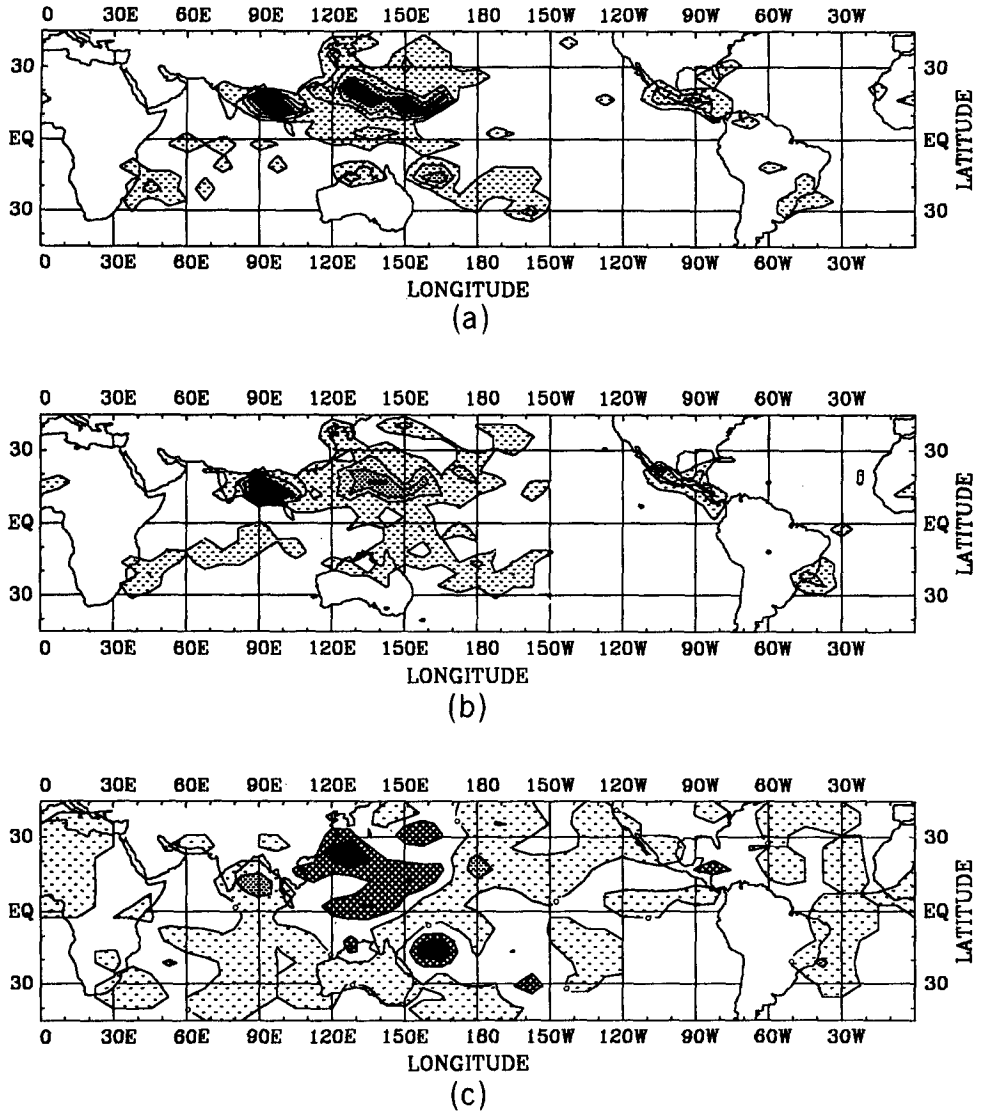

FIG. 12. Geographical distribution of the frequency of tropical-storm formation in the composite La Niña years (a) and El Niño years (b), and the difference between the two composites (c). For ease of comparison with Fig. 4, the values shown here are expressed in numbers of occurrences per 15 years. In panels (a) and (b), values within the ranges of 2–7, 7–12, and 12–17 are depicted by light, medium, and dense stippling, respectively. Regions with more than 17 occurrences are indicated by solid black. A nine-point space smoother has been used to construct panel (c). For the latter panel, light and medium stippling denote values of 0 to −2.5 and values less than −2.5, respectively; whereas values of 2.5–5 and values larger than 5 are indicated by crosshatching and solid black, respectively. Positive values in (c) indicate more TS formation during La Niña years.

might not be the direct result of such disturbances. In fact, Ding and Reiter (1983) found that when the WNP region experiences fewer typhoons, the rainfall over continental India is well below normal, whereas the monsoon rainfall over the Bay of Bengal itself is above normal. In other words, there seems to exist a positive relationship between monsoon rainfall over the Bay of Bengal and ENSO. Assuming that a large fraction of monsoon rainfall there is due to the development of TS systems, the positive correlation between ENSO and summertime TS formation over NIO, as found in the model, may not be unreasonable. However, further investigations of this relationship are evidently required.

5) OTHER OCEANS

The correlations between ENSO and TS formation over the South Atlantic and eastern North Atlantic are not significant. Over ESP, there is no TS formation both in the model and in observations. Over ENP, fewer TS are found in La Niña years (figure not shown). There seems to be a weak positive correlation between TS formation over ENP and the SST index. However, the correlation coefficients for different months and for the whole year are all below the 95% significance level.

To summarize the geographical dependence of the relationship between TS formation and ENSO, the data for TS formation in seven La Niña and six El Niño years have been extracted separately from the model record. The distributions of the mean frequency of TS formation for the cold and warm years are shown in Figs. 12a and 12b, respectively. For comparison with Fig. 4, the values shown here are the corresponding annual mean values at each grid point multiplied by 15. The difference between these two patterns is shown in Fig. 12c. To suppress small-scale features, a nine-gridpoint space smoother (Holloway 1958) has been applied to the difference field in Fig. 12c. The results indicate that, although the spatial patterns of TS formation for the warm and cold years are similar to each other, the frequency of TS formation over different oceans does change noticeably. For the whole globe, the annual frequency of TS formation is reduced from 77 in La Niña years to 65 in El Niño years. The decrease in frequency of TS formation in La Niña years occurs mainly over the Bay of Bengal and CNP and also over SIO and ENP. The increase in TS formation during La Niña years is discernible over WNP, WSP, and WNA. The variation of TS formation over WNP between the warm and cold episodes of ENSO is the strongest both in magnitude and areal extent. The polarity of the change in frequency of TS formation over WNP is opposite to that over CNP, thus confirming the existence of the seesaw in TS formation between WNP and CNP.

To further analyze the impact of ENSO on TS formation in individual months, the seasonal variations of the composite frequency of storm formation for warm and cold events are presented in Fig. 13. Results are shown only for those maritime areas where the frequency of TS formation in the period of May–November is significantly correlated with ENSO (Table 3). Over WNP (Fig. 13a), more TS are generated in La Niña years than in El Niño years in the periods of April to September and December to February. Observational analyses (Li 1988) show that the strongest neg-

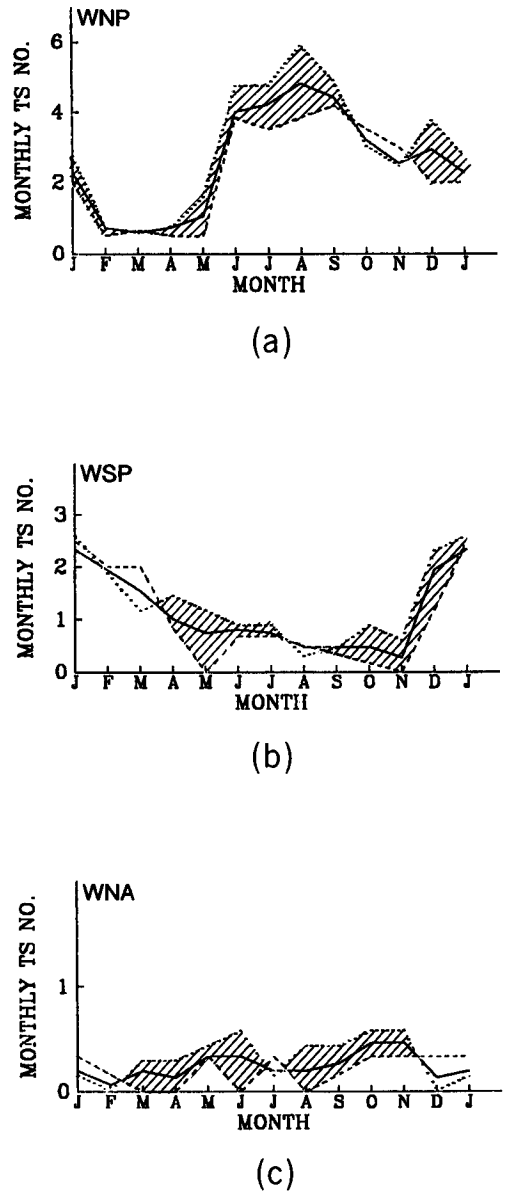

FIG. 13. Seasonal variation of the composite frequency of storm formation during individual calendar months in (a) WNP, (b) WSP, and (c) WNA. The composite values for warm El Niño and cold La Niña years are depicted by the dashed and dotted curves, respectively. The 15-yr mean frequency is depicted by the solid curves. Stippling indicates those months in which the number of tropical storms in La Niña years is more than that in El Niño years.

ative correlations between the frequency of TS formation and Pacific SST occur from July to November. Over WSP (Fig. 13b), the largest differences between the El Niño and La Niña years are found from September to December and also from April to June. The former period is in the early part of the Australian cyclone season (October–April). This result is in agreement with that inferred from the observations (Nicholls 1979).

5. ENSO composites of the large-scale flow

As discussed in section 1, TS are generated under certain favorable conditions in the local SST field as well as the ambient circulation pattern. In the present paper, only the influence of the large-scale flow field on TS formation will be investigated. The direct impact of different types of SST distribution on the atmospheric circulation and TS statistics will be considered in future experiments (see discussion in section 6). This section is devoted to a comparison of composite circulation charts for warm and cold phases of ENSO. The wind field has been decomposed into rotational and divergent components by computing the streamfunction and velocity potential, respectively. The results presented here are based on the boreal summer months (July–September). Results for the annual mean are very similar to the summer composites.

Figure 14 shows the difference between the La Niña and El Niño composites of simulated streamfunction and rotational wind at 950 and 200 mb. At 200 mb (Fig. 14a), two anomalous large-scale cyclones are found to straddle the equator over the central Pacific. Anticyclonic vorticity prevails over the remaining areas. Strong anomalous westerlies along the equator are simulated between 150°E and 120°W, while the rest of the equatorial zone is dominated by anomalous easterlies. The 950-mb difference field (Fig. 14b) is characterized by a spatial pattern similar to that for the 200-mb level, except for a sign reversal. The patterns shown here are reminiscent of the analytic solution of Gill (1980) for the atmospheric response to tropical heating symmetric about the equator. The anomalous anticyclonic vorticity at 950 mb over the central Pacific as well as the Bay of Bengal would tend to inhibit storm development during La Niña years. On the other hand, the anomalous cyclonic vorticity at 950 mb and anticyclonic vorticity at 200 mb over

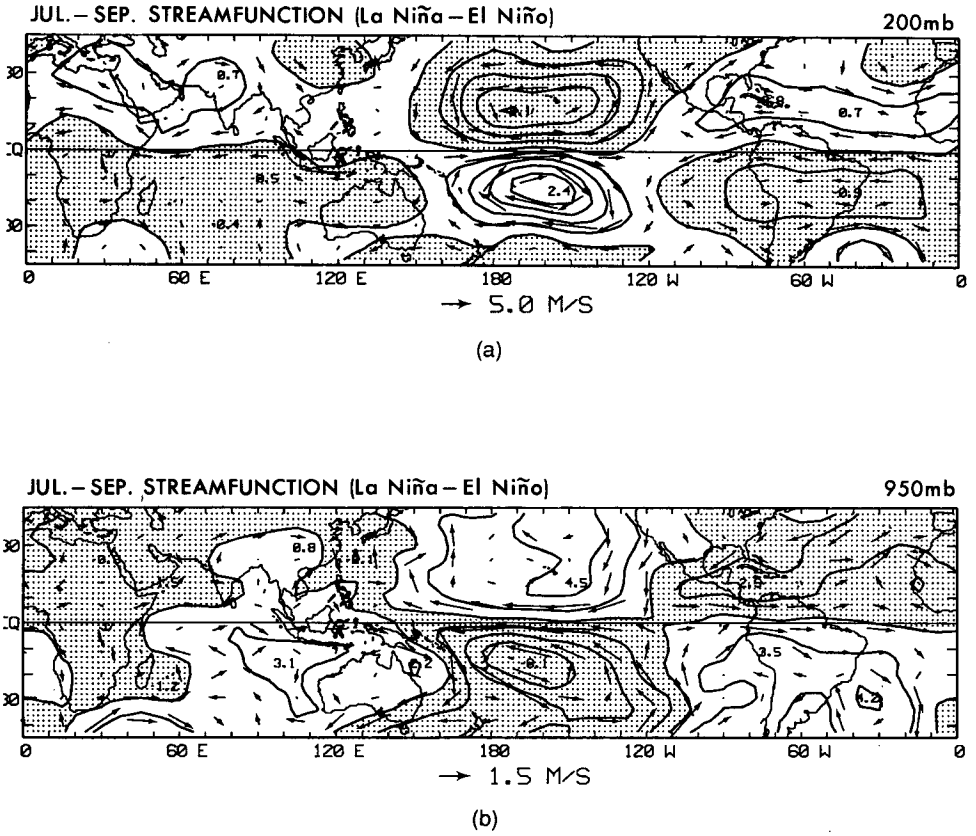

FIG. 14. Distribution of the difference between the La Niña and El Niño composites of simulated streamfunction and rotational wind vector at (a) 200 mb, contour interval for streamfunction: 5×10^6 m^2 s^{-1} and (b) 950 mb, contour interval: 2×10^6 m^2 s^{-1}, for the July–September period. The scale for the wind vectors is given at the bottom of each panel. Stippling indicates negative streamfunction.

much of the remaining maritime area should favor storm development during the cold events.

The difference charts of velocity potential and divergence wind, as shown in Fig. 15, are also characterized by a sign reversal between the lower and upper levels. The eastern Pacific comes under the influence of anomalous low-level divergence and upper-level convergence during La Niña. The anomalous low-level convergence over the Caribbean Sea, WNP, WSP, and the Indian subcontinent, together with anomalous divergence at 200 mb over the same sites, are in favor of local TS development during the cold events.

Considering the streamfunction and velocity potential composites together, it is seen that the WNP, WSP, and Caribbean regions are associated with anomalous convergence and cyclonic vorticity at the low level and with divergence and anticyclonic vorticity at the upper level during La Niña. These regions coincide with sites of above-normal frequency of TS formation during the cold events. On the other hand, the Bay of Bengal is associated with anomalous low-level anticyclonic vorticity during the same period. Below-normal storm frequency might then be expected during the cold events.

The seesaw of TS formation between WNP and CNP found in the last section can also be interpreted in light of the composite streamfunction and velocity potential patterns. In La Niña years at 950 mb, while anomalous cyclonic vorticity and convergence prevail in the WNP region, CNP is dominated by anomalous anticyclone vorticity and divergence. These circulation anomalies tend to enhance TS formation in WNP and suppress it in CNP.

Over the WNP region, an above-normal number of simulated storms (28 per year) is generated in the La Niña year of 1974, whereas the least frequent simulated storm development (18 per year) occurs in the El Niño year of 1972. In order to understand the difference in large-scale flow between the summers of these two years, the west–east cross section of the August mean wind field along 11.25°N is shown in Fig. 16. This latitude corresponds to the southern edge of the region of maximum storm frequency over WNP (see Fig. 4a). In 1974 (Fig. 16b), strong monsoon westerlies extend eastward from the Indian Ocean to WNP. These westerlies meet with the strong easterly trades at 150°E, and strong low-level convergence and rising motion are simulated at this longitude. The enhanced cyclonic vorticity and convergence associated with the deepening of the east Asia monsoon trough in this La Niña year are therefore conducive to storm formation. In

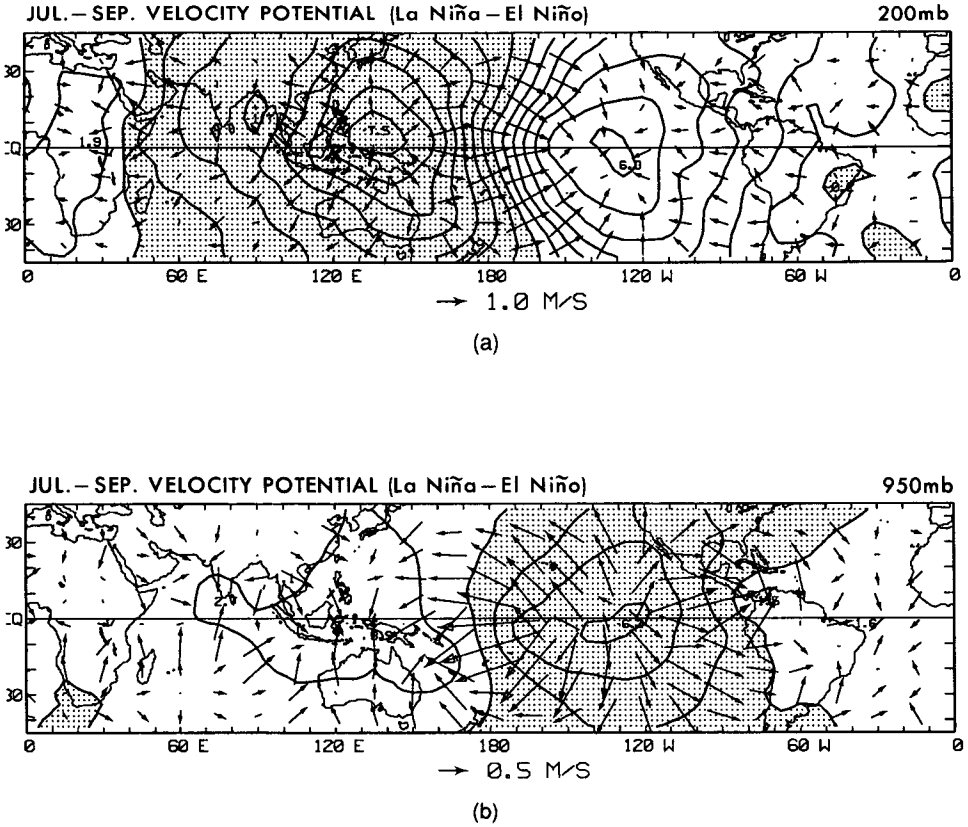

FIG. 15. As in Fig. 14, but for velocity potential and divergent wind vector. Contour intervals for the velocity potential are 1×10^6 m^2 s^{-1} and 2×10^6 m^2 s^{-1} for the 200- and 950-mb levels, respectively.

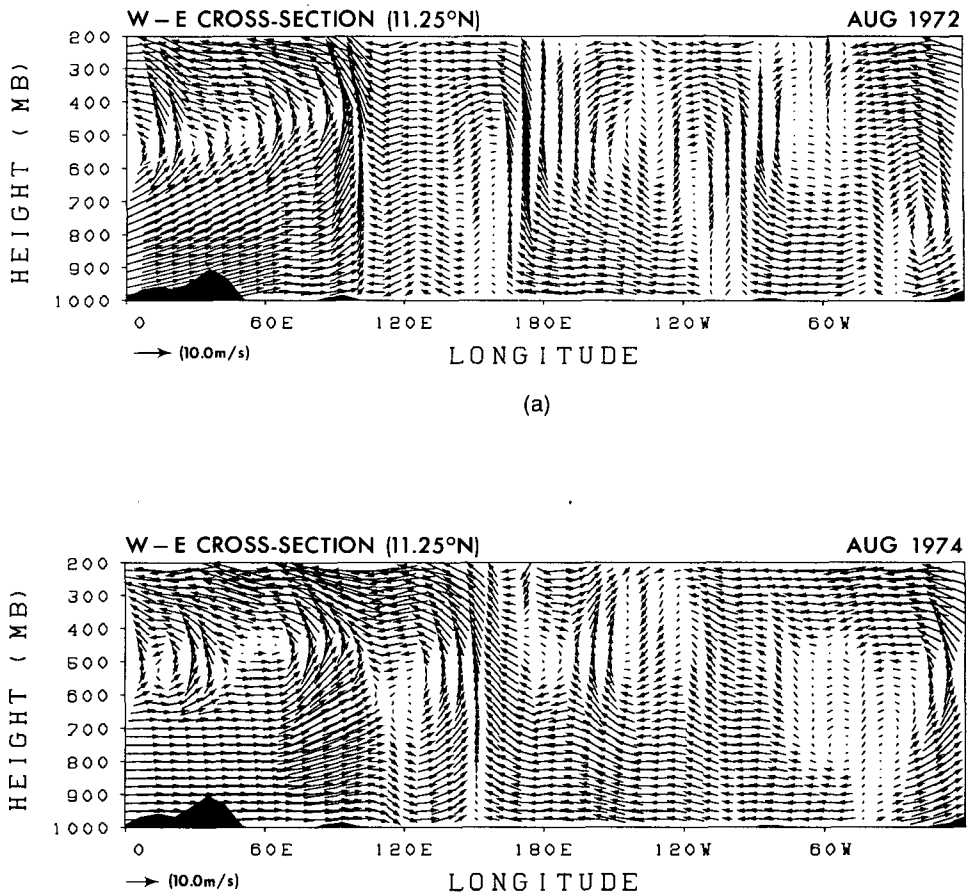

FIG. 16. Longitude–pressure distribution of the circulation at 11.25°N in (a) August 1972 and (b) August 1974. For better visualization of the circulation pattern, the vertical component of the wind vector has been multiplied by a factor of 2000 before plotting. The scale for the resultant wind vector thus obtained is given at the lower left-hand corner of each panel.

the El Niño year of 1972 (Fig. 16a), as the warm SST anomaly migrates eastward, the strong rising center over the western Pacific is also shifted toward the dateline. At the same time, the monsoon westerlies over south Asia are weakened and terminated at the Gulf of Siam (105°E), thus resulting in a second rising center there. In the WNP region west of 160°E, no apparent low-level convergence or large-scale ascent is discernible. This environment is not favorable for storm development in the WNP region (Frank 1987).

Figure 17 shows the north–south cross sections of the wind field for 1972 and 1974 along 142.5°E, which corresponds to the longitude of maximum frequency of storm formation. In the La Niña year of 1974 (Fig. 17b), cross-equatorial southerlies prevail over the low latitudes, resulting in rising motion over the entire 10°–30°N zone. On the other hand, in the El Niño year of 1972 (Fig. 17a), the cross-equatorial southerlies meet with the northerlies at about 12°N in the lower troposphere. However, the ascent associated with this convergence is weak, and upper-layer sinking is simulated over the same region, so that the meridional flow turns toward the equator near 700 mb, and the strongest ascent in the upper troposphere occurs at 0°–10°S.

The features revealed by the above case study are also discernible from the composites shown in Figs. 14 and 15. During La Niña years, intensified near-equatorial easterlies at 950 mb prevail over much of the Pacific. At the same time, enhanced surface westerlies occur in the equatorial zone extending from the western Indian Ocean to the Indonesian archipelago. These model results agree with those from observational analyses performed by Angell (1981) and Rasmusson and Carpenter (1982).

It is known from various observational studies that, during El Niño years, the warm waters of the western tropical Pacific migrate eastward, leading to the shifting of the heating center toward the date line (Lau and Chan 1985, 1986; Sardeshmukh and Hoskins 1985). The forced circulation in the equatorial zonal plane associated with this heating center will also be displaced eastward, resulting in the intensification of surface easterlies over the Americas and of surface anticyclonic

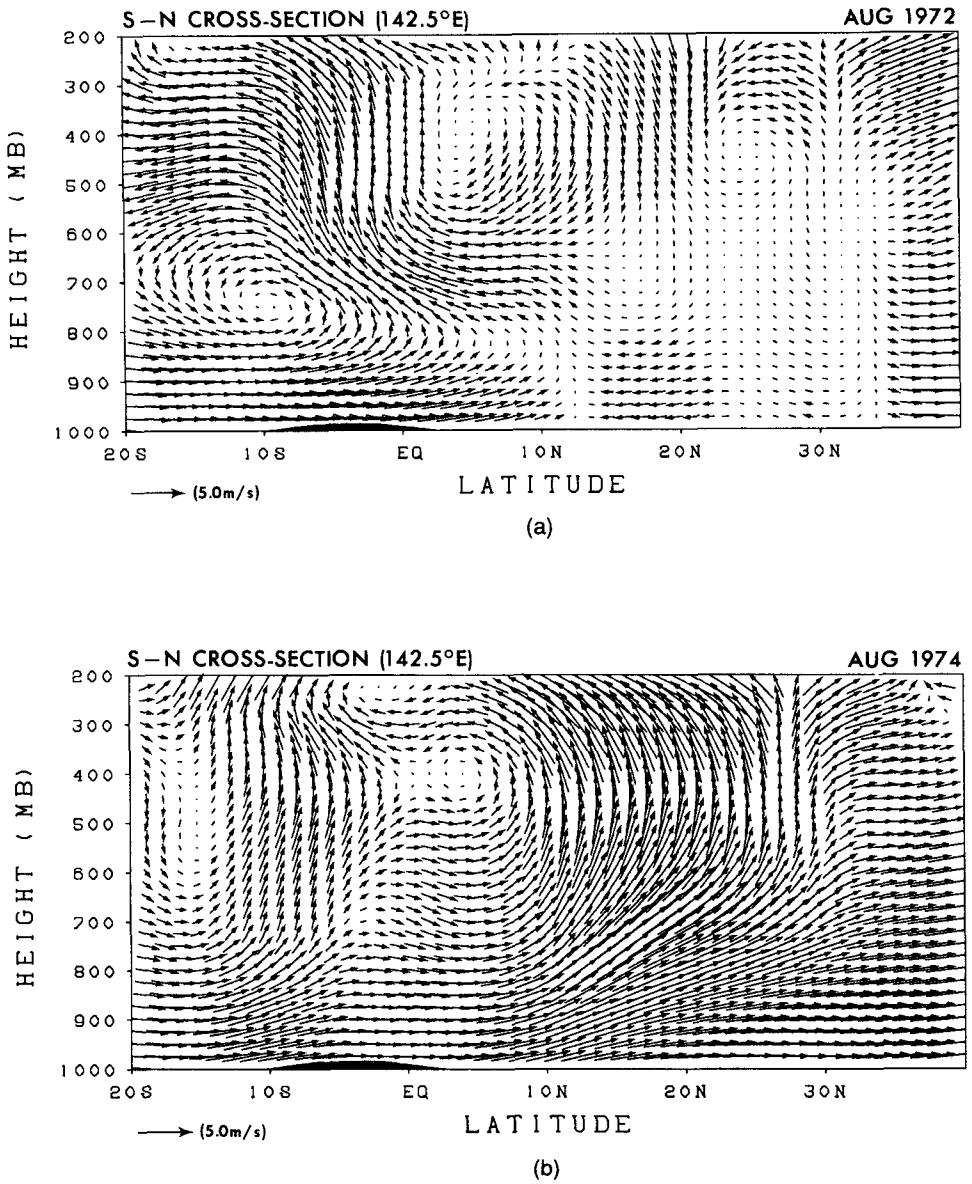

FIG. 17. Latitude–pressure distribution of the circulation at 142.5°E, in (a) August 1972 and (b) August 1974. For better visualization of the circulation pattern, the vertical component of the wind vector has been multiplied by a factor of 750 before plotting. The scale for the resultant wind vector thus obtained is given at the lower left-hand corner of each panel.

vorticity over WNA. The upper-level outflow from the heating area also enhanced the equatorial upper westerlies in the central American region (Arkin 1982), so that the 200-mb anticyclonic vorticity over WNA is weakened. These developments in the observed ambient flow structure in the North Atlantic sector are accompanied by a reduction in TS activity in this region during El Niño and are reproduced well in the model (see Figs. 14–17). It seems that the interannual variation of TS activity in the WNA is mostly related to the longitudinal displacement of the Walker circulation during El Niño and La Niña events.

6. Conclusions and discussions

In spite of the coarse resolution of the GCM used for this study, it is demonstrated that typhoonlike events do occur in the course of the experiment. The large-scale structure of the TS appearing in the model atmosphere bears considerable resemblance to the observed characteristics. The model disturbances examined here have a smaller vertical extent and generally have lower intensities than the corresponding features in the observed atmosphere or in simulations using models with much finer meshes.

The geographical distribution and seasonal variation of TS formation simulated by the model are similar to the corresponding observational results. The most favorable region for TS formation is the WNP region east of the Philippines. Other sites of enhanced storm activity are WSP, the eastern part of the Bay of Bengal, WNA, and SIO. Most of the TS occur in the warm half of the seasonal cycle.

Over the WNA, WNP, and WSP regions, more TS are simulated in La Niña years than in El Niño years. This relationship is particularly evident in the summer months in WNP and WNA, and in spring and early summer in WSP. These model results agree with observations. In the Indian Ocean, the correlation between TS activity and ENSO seems to be seasonally dependent. In El Niño years, above-normal storm activity is simulated in summer, and below-normal activity occurs in winter. The reverse situation applies to La Niña years. The latter results remain to be substantiated by more detailed investigations of observational data.

In La Niña years, the Walker circulation shifts westward, resulting in stronger rising motion over the Indonesian archipelago. At the same time, the monsoon trough and the associated westerlies extending from the Indian Ocean to the western Pacific are intensified. The strengthened convergence and cyclonic vorticity along the monsoon trough are accompanied by an enhancement of TS activity over WNP and WSP. In El Niño years, as the convective heating over the equatorial Pacific shifts eastward, above-normal low-level convergence and upper-level divergence occur over the eastern Pacific. In the South American sector, low-level equatorial easterlies and high-level westerlies are simulated, resulting in the weakening of low-level cyclonic vorticity and convergence, and upper-level anticyclonic vorticity and divergence over the tropical WNA. The frequency of TS formation in WNA during warm events is accordingly lowered.

In connection with ENSO, there exists a seesaw in TS formation frequency between WNP and CNP. This can also be explained by the anomalous tropical circulation. In La Niña years, low-level equatorial easterlies over the central Pacific and equatorial westerlies over the eastern Indian Ocean and the western Pacific Ocean are intensified. Enhanced low-level convergence and cyclonic vorticity occur over WNP, while a strong anticyclone associated with divergence dominates CNP. The polarity of the anomalous circulation at the upper level is opposite to that at the lower level. Therefore, during La Niña years, more TS tend to develop over WNP, whereas their appearance over CNP is suppressed.

The present study reveals the existence of significant correlations between TS formation over several maritime areas and ENSO. These relationships are then interpreted in terms of the changes in the large-scale tropical circulation during warm and cold events. However, the mechanisms contributing to such correlations require further study. Numerical experiments by Keshavamurty (1982) have shown that the tropical atmospheric response to equatorial SST anomalies is sensitive to the location of the anomaly relative to the ascending and descending branches of the Walker circulation. The results from the latter experiments and the evidence provided in the present study suggest that the geographical location and spatial pattern of the imposed SST anomaly may have a significant impact on the frequency of TS formation. To better understand the mechanisms linking ENSO events to TS formation, as well as the sensitivity of TS formation to various spatial configurations of the SST anomalies, several additional experiments incorporating different types of SST anomaly patterns have recently been launched at GFDL. Analysis of these new integrations will hopefully shed further insights on the role of perturbations at various ocean sites in altering the variability of TS occurrence.

Acknowledgments. We are indebted to S. Manabe for proposing this topic of research and for valuable suggestions. We would like to thank A. Broccoli for sharing his experience in detecting and analyzing TS using GCM output and for many interesting discussions. Thanks are also due to Y. Kurihara for offering many useful suggestions. The careful reviews of our first draft by all three aforementioned colleagues were indispensable for the improvement of this paper. We are grateful to G. Philander and R. Tuleya for interesting discussions on this study. The first author wishes to express his gratitude to J. Mahlman and other colleagues at GFDL and at the Program of Atmospheric and Oceanic Sciences, Princeton University, for their assistance during his visit at Princeton.

REFERENCES

Angell, J. K., 1981: Comparison of variations in atmospheric quantities with sea surface temperature variations in the equatorial eastern Pacific. *Mon. Wea. Rev.*, **109**, 230–243.

Anthes, R. A., 1982: Tropical cyclones, their evolution, structure, and effects. *Meteor. Monogr.*, No. 41, Amer. Meteor. Soc., 208 pp.

Arkin, P. A., 1982: The relationship between interannual variability in the 200 mb tropical wind field and the Southern Oscillation. *Mon. Wea. Rev.*, **110**, 1393–1404.

Bengtsson, L., H. Bottger, and M. Kanamitsu, 1982: Simulation of hurricane-type vortices in a general circulation model. *Tellus*, **34**, 440–457.

Bjerknes, J., 1966: A possible response of the atmospheric Hadley circulation to equatorial anomalies of ocean temperature. *Tellus*, **18**, 820–829.

——, 1969: Atmospheric teleconnections from the equatorial Pacific. *Mon. Wea. Rev.*, **97**, 163–172.

Blackmon, M. L., J. E. Geisler, and E. J. Pitcher, 1983: A general circulation model study of January climate anomaly patterns associated with interannual variation of equatorial Pacific sea surface temperatures. *J. Atmos. Sci.*, **40**, 1410–1425.

Broccoli, A. J., and S. Manabe, 1990: Can existing climate models be used to study anthropogenic changes in tropical cyclone climate? *Geophys. Res. Lett.*, **17**, 1917–1920.

Burpee, R. W., 1974: Characteristics of North African easterly waves

during the summer of 1968 and 1969. *J. Atmos. Sci.*, **31**, 1556–1570.

Carlson, T. N., 1969: Synoptic histories of three African disturbances that developed into Atlantic hurricanes. *Mon. Wea. Rev.*, **97**, 256–276.

Chan, J. C. L., 1985: Tropical cyclone activity in the Northwest Pacific in relation to the El Niño/Southern Oscillation phenomenon. *Mon. Wea. Rev.*, **113**, 599–606.

——, 1990: The influence of sea-surface temperatures on tropical cyclone activity in the western North Pacific. *Abstracts of the Int. TOGA Scientific Conf.* Honolulu, HI.

Chen, L. and Y.-H. Ding, 1979: *On West Pacific Typhoon.* Chinese Science Press, 491 pp. (in Chinese)

Ding, Y.-H., and E. R. Reiter, 1981: Some conditions influencing the variability in typhoon formation over the west Pacific Ocean. *Arch. Meteor. Geophys. Bioklim.*, **A30**, 327–342.

——, and ——, 1983: Large-scale hemispheric teleconnections with the frequency of tropical cyclone formation over the northwest Pacific and North Atlantic Ocean. *Arch. Meteor. Geophys. Bioklim.*, **A32**, 311–337.

Dong, K., 1988: El Niño and tropical cyclone frequency in the Australian region and the northwest Pacific. *Aust. Meteor. Mag.*, **36**, 219–255.

Frank, W. M., 1977: The structure and energetic of the tropical cyclone, Paper I: Storm structure. *Mon. Wea. Rev.*, **105**, 1119–1135.

——, 1987: Tropical cyclone formation. *A Global View of Tropical Cyclones,* R. L. Elsberry, W. M. Frank, G. J. Holland, J. D. Jarrell, and R. L. Southern, Eds., 53–90.

Gill, A. E., 1980: Some simple solutions for heat-induced tropical circulation. *Quart. J. Roy. Meteor. Soc.*, **106**, 447–462.

Gray, W. M., 1968: Global view of the origin of tropical disturbances and storms. *Mon. Wea. Rev.*, **96**, 669–700.

——, 1977: Tropical cyclone genesis in the western North Pacific. *J. Meteor. Soc. Japan*, **55**, 465–481.

——, 1979: Hurricanes: Their formation, structure and likely role in the tropical circulation. *Meteorology over the Tropical Oceans,* D. B. Shaw, Ed., Roy. Meteor. Soc., 155–218.

——, 1984a: Atlantic seasonal hurricane frequency: Part I: El Niño and 30 mb quasi-biennial oscillation influences. *Mon. Wea. Rev.*, **112**, 1649–1668.

——, 1984b: Atlantic seasonal hurricane frequency. Part II: Forecasting its variability. *Mon. Wea. Rev.*, **112**, 1669–1683.

——, P. Mielke, and K. Berry, 1987: Statistical analysis of Gray's Atlantic seasonal hurricane forecast scheme. *17th Conf. on Hurricanes and Tropical Meteorology,* Miami, Amer. Meteor. Soc., 227–230.

Holloway, J. L., 1958: Smoothing and filtering of time series and space fields. *Advances in Geophysics,* vol. 4, Academic Press, 351–389.

Keshavamurty, R. N., 1982: Response of the atmosphere to sea surface temperature anomalies over the equatorial Pacific and the teleconnections of the Southern Oscillation. *J. Atmos. Sci.*, **39**, 1241–1259.

Krishnamurti, T. N., D. Oosterhof, and N. Dignon, 1989: Hurricane prediction with a high resolution global model. *Mon. Wea. Rev.*, **117**, 631–669.

Kurihara, Y., and R. E. Tuleya, 1981: A numerical simulation study on the genesis of a tropical storm. *Mon. Wea. Rev.*, **109**, 1629–1653.

Lau, K. M., and P. H. Chan, 1985: Aspects of the 40–50 day oscillation during the northern winter as inferred from outgoing longwave radiation. *Mon. Wea. Rev.*, **113**, 1889–1909.

——, and ——, 1986: The 40–50 day oscillation and the El Niño/Southern Oscillation: A new perspective. *Bull. Amer. Meteor. Soc.*, **67**, 533–534.

Lau, N.-C., 1985: Modeling the seasonal dependence of the atmospheric response to observed El Niños in 1962–76. *Mon. Wea. Rev.*, **113**, 1970–1996.

Li, Congyin, 1988: Actions of typhoon over the western Pacific (including the South China Sea) and El Niño. *Adv. Atmos. Sci.*, **5**, 107–115.

Manabe, S., J. L. Holloway, Jr., and H. M. Stone, 1970: Tropical cyclone in a time-integration of a global model of the atmosphere. *J. Atmos. Sci.*, **27**, 580–613.

Mandal, G. S., 1989: Low frequency oscillations and seasonal variability of tropical cyclones in north Indian Ocean. *Second Int. Workshop on Tropical Cyclones (IWTC-II),* Manilla, WMO/TP No. 319, WMO/CAS/OFDA, 341–354.

Nicholls, N., 1979: A possible method for predicting seasonal tropical cyclone activity in the Australian region. *Mon. Wea. Rev.*, **107**, 1221–1224.

——, 1984: The Southern Oscillation, sea-surface temperature, and interannual fluctuations in Australian tropical cyclone activity. *J. Climatol.*, **4**, 661–670.

Palmer, T. N., and D. A. Mansfield, 1984: Response of two atmospheric general circulation models to sea-surface temperature anomalies in the tropical east and west Pacific. *Nature,* **310**, 483–485.

Pan, Y. H., 1982: The effect of the thermal state of equatorial eastern Pacific on the frequency of typhoon over western Pacific. *Acta Meteorol. Sin.* **40**, 24–34 (in Chinese with English abstract).

Philander, S. G. H., 1989: *El Niño, La Niña, and the Southern Oscillation.* Academic Press, 293 pp.

Ramage, C. S., and A. M. Hori, 1981: Meteorological aspects of El Niño. *Mon. Wea. Rev.*, **109**, 1827–1835.

Rasmusson, E. M., and T. H. Carpenter, 1982: Variations in tropical sea surface temperature and surface wind fields associated with the Southern Oscillation/El Niño. *Mon. Wea. Rev.*, **110**, 354–384.

——, and T. H. Carpenter, 1983: The relation between eastern equatorial Pacific sea surface temperatures and rainfall over India and Sri Lanka. *Mon. Wea. Rev.*, **111**, 517–528.

——, and J. M. Wallace, 1983: Meteorological aspects of the El Niño/South Oscillation. *Science,* **222**, 1195–1202.

Rowntree, P. R., 1972: The influence of tropical east Pacific Ocean temperature on the atmosphere. *Quart. J. Roy., Meteor. Soc.*, **98**, 290–321.

Sardeshmukh, P. D., and B. J. Hoskins, 1985: Vorticity balances in the tropics during the 1982–1983 El Niño–Southern Oscillation event. *Quart. J. Roy. Meteor. Soc.*, **111**, 261–278.

Shea, D. J., and W. M. Gray, 1973: The hurricane's inner core region: I. Symmetric and asymmetric structure. *J. Atmos. Sci.*, **30**, 1544–1564.

Shukla, J., and D. A. Paolino, 1983: The Southern Oscillation and long-range forecasting of the summer monsoon rainfall over India. *Mon. Wea. Rev.*, **111**, 1830–1837.

——, and J. M. Wallace, 1983: Numerical simulation of the atmospheric response to equatorial Pacific sea surface temperature anomalies. *J. Atmos. Sci.*, **40**, 1363–1392.

Wang, Z. L., and L. Fei, 1987: *Handbook of Typhoon Forecasts.* Chinese Meteorology Press, 360 pp. (in Chinese.)

Wu, Guoxiong, and U. Cubasch, 1987: The impact of El Niño anomaly on mean meridional circulation and transfer properties of the atmosphere. *Sci. Sin. (B),* **30**, 533–545.